Geophysical and geochemical constraints on the age and paleoclimate implications of two Holocene lacustrine cores from the headwater region of the Claro River, Elqui Province, Coquimbo Region, Chile

By

Rachel J. Tiner, B.S.

A Thesis Submitted to the Department of Geological Sciences

California State University, Bakersfield

In Partial Fulfillment for the Degree of

Masters of Science in Geology

Spring 2016

Geophysical, and geochemical constraints on the age and paleoclimate implications of two Holocene lacustrine cores from the headwater region of the Claro River, Elqui Province, Coquimbo Region, Chile

By

Rachel J. Tiner

This thesis has been accepted on the behalf of the Department of Geological Sciences by their supervisory committee:

Robert Negrini, Ph.D.
Committee Chair

Junhua Guo, Ph.D.

Jose L. Antinao, Ph.D.

Acknowledgements

This project was funded by the National Science Foundation, USA: NSF EAR Award #1349416: Millenial variability of hillslope dynamics and alluvial aggradation in semiarid regions: a view from the southern hemisphere and NSF HRD Award #1137774: California State University, Bakersfield Center for Research in Science and Technology (NSF CSUB CREST)

I would like to acknowledge those who were responsible for coring of the two lakes studied in this project: Antonio Maldonado, Eugenia de Porras, Daniela Cardenas, and Jan Wowrek of the Centro de Estudios Avanzados en Zonas Aridas (CEAZA), La Serena, Chile.

I would also like to acknowledge those who assisted me with sampling, sample preparation, and sample analysis: Elizabeth Powers, Karol Casas, Maryanne Bobbitt, Sarah Brown, and Morgan Kayser of California State University, Bakersfield (CSUB).

I would also like to acknowledge Ken Verosub for his instruction and guidance in using the 2G Enterprises Rock Magnetometer.

I would like to thank Antonio Maldonado for his advice and insights through conception and completion of this project.

I would like to thank Jose Luis Antinao for writing the grant proposal to fund this project and for his support and advice in the completion of the project.

I would also like to thank my advisor, Rob Negrini, for his support and advice through my Master's Degree and for being the one to first encourage me to pursue my Bachelor's Degree in geology and, later, my Master's Degree.

I am deeply grateful to my friends for their consistent presence in the Geology Department and personal and academic support through my Master's Degree: Nick Moreno, Alana Crown, Eric Heaton, Alyssa Kaess, and Linda Anderson.

Finally, I am also deeply grateful to my boyfriend, Zachary Martindale, for his consistent and whole-hearted support through my Master's Degree.

Abstract

A Holocene paleoclimate record for northern central Chile has been constructed using two lacustrine cores from the high-elevation Andes at ~30° S latitude. The 1.37-m Laguna Cerritos Blancos (LCB) core has been dated from 0-4.0 cal kyr BP using paleomagnetic secular variation (PSV) and ^{14}C radiometric dating and the 5.53-m Laguna El Cepo (LEC) from 0-10.9 cal kyr BP using ^{14}C radiometric dating. Coarser grain sizes, bimodal grain-size distributions, greater carbon and nitrogen weight percentages, and C/N ratios were found to co-vary suggesting increased storm activity and wet climate. The Holocene began with a wet period from ~10.9-9.5 cal kyr BP, then dry conditions beginning ~9.5 cal kyr BP with a transition to wetter conditions from ~8.3 until ~7.7 cal kyr BP. ~7.7-5.5 cal kyr BP is an arid period, then moisture and storm activity increase gradually from ~5.5 to ~4.9 cal kyr BP when conditions remain mildly dry until 4.4 cal kyr BP. Moisture and storm activity increase abruptly from ~4.0 cal kyr BP to ~3.8 cal kyr BP when moisture decreases gradually into a dry period from ~2.6 until 2.2 cal kyr BP wherein moisture and storm activity increase. A slight decrease in moisture after ~0.3 cal kyr BP is probably consistent with the current dry conditions in the study area. This paleoclimate record is consistent with others of the region. Accordingly, the wet periods with greater storm activity are likely caused by the prevalent influence of the westerlies, while stable and dry conditions are probably the result of the dominant influence of the Southeast Pacific anticyclone (SPA). Furthermore, the intervals of increased storm activity observed in the Chilean lake records correlate to a first order with short periods of global rapid climate change, including the 8.2 ka event.

Table of Contents

1. Introduction

Norte Chico is an important agricultural region in north-central Chile that is known for producing export-quality wine and distilled spirits (pisco). The water supply of this region has been strained over recent decades due to increased agricultural activity coupled with increased drought (Meza, 2013). The main objective of this project is to build a well-dated, Holocene paleoclimate record that can be used as input to assess landscape responses to expected climate change in the near future.

Northern central Chile lies between the dominant circulation features affecting western South America making it ideal for paleoclimate study because even relatively small latitudinal variations in these circulation systems (e.g., Garreaud, 2009) should be reflected in paleoclimate records from the area. Presented here are such records based on two Holocene-aged lacustrine cores from the high-elevation Chilean Andes used to constrain the duration and timing of climate shifts hypothesized in previous paleoclimate studies from the region.

Veit (1996) described and compiled soils, lacustrine, and alluvial fan depositional records throughout northern central Chile to determine paleoclimate conditions. Cover sediment deposition near the coast and alluvial fan deposition in the Andes were used as evidence to suggest landscape instability caused by frequent storm activity, while soil development on the coast and peat bog and soil development in the Andes suggested a more stable landscape as a result of decreased storm activity. Until 7.3 cal kyr BP conditions were wet, then became drier until 5.1 cal kyr BP. Precipitation increased from 5.1 to 3.7 cal kyr BP, decreased 3.7 to 3.0 cal kyr BP, then increased again after 3.0 cal kyr BP while also varying more frequently.

Building on the Veit (1996) study, Maldonado and Villagrán (2006) analyzed a swamp forest pollen record on the coast of northern Chile at ~32° S latitude and 100 m elevation to infer

paleoclimate for the past 9.9 cal kyr BP. To a first order, these two records found similar climate histories for the region, despite the use of very different evidence The record of Maldonado and Villagrán (2006) suggests that in the early Holocene, wet conditions prevailed, then a shift to aridity took place ~8.7-7.8 cal kyr BP. Increasingly pollen-starved sediment suggested that aridity increased in the interval from ~7.8-5.7 cal kyr BP. A return to humid conditions began after 5.7 cal kyr BP culminating at 4.2 cal kyr BP reflected in a significant increase in pollen and bulk organic content. From 3.0 to 2.2 cal kyr BP milder but arid conditions existed, the peak of which occurred at 2.75 cal kyr BP. At 2.2 cal kyr BP, a period of variable precipitation began with overall humid conditions, persisting until 1.3 cal kyr BP.

2. The Study Region

The area of study is located in the Elqui province of the Coquimbo Region in Chile. The Laguna Cerritos Blancos (LCB) and Laguna El Cepo (LEC) core locations lie within northern central semiarid Chile south of the hyperarid Atacama Desert and north of the Mediterranean climate zone of central Chile (Figure 1). Currently, the headwater area receives up to 200-300 mm annual precipitation (Oyarzún et al., 2013). The two lakes lie in the headwater region of the Elqui River. LCB is located at 30.429567° S, 70.238810° W and 3850 masl and is ~300 m in diameter. LEC is located at 30.264389° S, 70.301331° W and 2920 masl and is ~200 m in diameter. LEC is 19.3 km north-northwest of LCB. These two lakes lie within the southern portion of the Elqui river catchment. LCB drains into the Claro River, which then joins the Elqui River and is located 63 km east-northeast of the town of Vicuña. LEC lies within the headwaters of the Cochiguaz River, which feeds into the Claro River (Figure 2). The bedrock geology of the study area consists primarily of intrusive plutonic rocks that have been assigned locally to the El

Volcán unit composed of coarse grained, cataclastic biotite granites and the El León unit composed of medium grained, pink, biotite monzogranites (Mpodozis and Kay, 1992).

3. Methods

Two cores were extracted from the study area using a Livingstone-type, drive-rod piston corer. 271 samples were taken from the top 5.53 meters below ground surface (mbgs) of LEC, which consists of 6 drives and 60 samples were taken from the top 1.37 mbgs of LCB, which consists of 5 drives. Each core was sampled at 2 cm intervals and each sample was placed in a plastic box 5.13 cm^3 in volume, and oriented with respect to the presumably vertical axis of the core.

Lithological descriptions were conducted by Katharina Lehner at the Centro de Estudios Avanzados en Zonas Aridas (CEAZA) at the Universidad de La Serena, La Serena, Chile. The color, grain size, and other distinguishing characteristics of each layer were described to a resolution of 0.5 cm.

Fourteen AMS ^{14}C dates were obtained from samples taken from both cores (Figure 3). From the LCB core, 4 radiocarbon dates were obtained from bulk sediment samples. From the LEC core, 4 radiocarbon dates were obtained from charcoal samples and 6 were obtained from bulk sediment samples, 4 of which were obtained from the same intervals as the 4 charcoal samples. These samples were processed at the Center for Accelerator Mass Spectrometry at Lawrence Livermore National Laboratory. All dates were calibrated using CALIB rev7.1.0 and the data set SHCAL13.14c (Stuiver and Reimer, 1993). For all ^{14}C age models, the midpoint of the entire range of all 1σ ages was used (Table 1).

All magnetic measurements were performed on discrete samples. Low-field magnetic susceptibility was measured using a Bartington MS2 magnetic susceptibility meter with an

MS2B bottle sensor. Paleomagnetic secular variation (PSV) was attempted on both cores as a method of age control and was determined by measuring the natural remanent magnetization (NRM) using a 2G Enterprises Model 755 Rock Magnetometer at the University of California, Davis after alternating field demagnetization (AFD) at 0, 5, 10, 15, 20, 25, 30, 40, 60, 80, and 100 mT. A characteristic remanent magnetization (ChRM) was determined by applying principal component analysis (PCA) to the AFD measurements using ZPlotit software (Version 2009-10) written by G. Acton.

Anhysteretic remanent magnetization (ARM), imparted with bias field of 0.05 mT superimposed on an alternating field peaking at 100 mT, and isothermal remanent magnetization (IRM) at 1.0 T, were measured after AFD at 0, 10, 20, 30, 40, 60, 80, and 100 mT. The ratio IRM_{0mT}/ARM_{20mT} was calculated using IRM and ARM magnetizations after they were subjected to AFD at 0 and 20 mT, respectively. This ratio is often used to indicate magnetic grain size (Evans and Heller, 2003). The S-ratio (IRM_{300mT}/ IRM_{1000mT}) was calculated after IRMs were imparted on each sample in a forward induction of 1000 mT (IRM_{1000mT}) and an oppositely directed induction of 300 mT (IRM_{300mT}). The S-ratio is used to infer the amount of magnetite relative to hematite because magnetite saturates below fields of 300 mT (Evans and Heller, 2003). Similarly, the quantity of "hard" isothermal remanent magnetization (HIRM) [(IRM_{-300mT} + IRM_{1000mT})/2] is an indicator of the amount of hematite (Rosenbaum et al., 1996; Liu et al., 2007).

Grain size was analyzed using a Malvern Mastersizer 2000 at California State University, Bakersfield. Each sample was soaked in a mixture of deionized water and hexametaphosphate (calgon) for 24 hours, sieved to <1 mm to prevent system clogging, then sonicated for 5 minutes. The bulk grain size and coarse fraction grain size procedures were performed on each sample: 1)

a splitter aliquot was used to reach optimal laser obscuration as explained in Sperrazza et al. (2004), which produces the bulk mean grain size, then 2) the remaining sample was allowed to settle for 1.5 minutes, the water and suspended sediment was siphoned off, then the remaining heavy grains (coarse fraction) were analyzed similar to the procedure outlined in Blunt and Negrini (2015). The mean grain sizes, and clay, silt, and sand percentages were calculated. In addition, the grain-size value corresponding to the peak value of each grain-size distribution was identified to determine whether the mean grain size was convolved with a widely-distributed or poorly-sorted sample. These selected values will be referred to as the bulk and coarse fraction grain-size populations. The greater the difference between the bulk and coarse fraction mean and population grain size values, the greater degree of bimodality the sample has.

Total weight percent nitrogen (N) and total weight percent carbon (C) were measured to a sensitivity of >10 ppm with a Costech 4010 Elemental Analyzer at California State University, Bakersfield. 20 mg of sample was homogenized and dried at 105°C for 24 hours, then added to a tin cup in which it was combusted and measured through gas chromatography. Total inorganic carbon (TIC) was determined through carbon coulometry where CO_2 is released from the sample by acidification in a UIC CM5230 Acidification Module and measured through a titration reaction in a UIC model 5020 Carbon Coulometer CM150 to a sensitivity of 1µg. TIC was subtracted from the C to obtain the total organic carbon (TOC). In the case of this study, weight percent TIC was usually negligible. Because the TIC was negligible the C was considered to be equal to the TOC and was used to calculate the C/N ratio. The C/N ratios were then converted to molar ratios according to McFadden et al. (2005).

4. Paleoclimate Proxies

4.1 Grain Size Analysis

Detrital grain size can be used as a proxy for relative lake depth. For example, the coarse fraction mean grain size has been used to indicate the occurrence and relative intensity of flooding events (e.g., Kirby et al., 2012). In the Elqui River headwaters, sediment is largely moved by storm activity (Ortega et al., 2012) or springtime snowmelt run-off (Veit, 1996). In the high-elevation Andes, alluvial fans have been interpreted to be a result of increased storm activity and average precipitation, while the development of peat bogs and soils have been interpreted to be a result of decreased precipitation and humidity. Furthermore, essentially all precipitation above 3000 masl today falls as snow, thus alluvial fan deposition at this elevation is interpreted to be a result of springtime snowmelt run-off (Veit, 1996). Accordingly, larger average grain sizes and greater spreads between bulk and coarse fraction mean and population grain sizes within each distribution or greater bimodality of the samples will be interpreted as an increase in storm activity and moisture.

4.2 Geochemical Analyses

The geochemical contents of lake sediments, particularly carbon and nitrogen, can be indicators of the biological productivity occurring in and around it. The organic carbon to nitrogen ratios (C/N) often show whether terrestrial or aquatic plant matter is dominant in the lake (Cohen, 2003). Since organic carbon with high C/N values in lakes is largely the product of terrestrial plants that arrive in the lake due to increased discharge (Meyers and Lallier-Verges, 1999), C/N ratios can also be used as a proxy for relative discharge into the lake (Kirby, 2012). Inorganic carbon is usually a product of precipitated carbonate due to increased salinity caused by lake shallowing (Cohen, 2003).

5. Results

5.1 Laguna Cerritos Blancos

5.1.1 Age Control

5.1.1.1 Radiocarbon Dates

The bulk sediment radiocarbon ages from LCB core yield a sedimentation rate of ~0.3 m/kyr. Extrapolating the 4 radiocarbon ages, dates the bottom of the core at ~4.5 ^{14}C cal kyr BP (Figure 3).

5.1.1.2 Paleomagnetic Secular Variation

The anchored (ANC) PCA method was used to construct the LCB PSV record. This method removes outliers and finds the best-fit line through the data while anchoring the line to the origin (Acton, 2009). 11 samples were removed from the LCB PSV record because they did not possess pseudo-exponentially decaying magnetizations after each AFD level, nor a stable ChRM indicated by similar inclination and similar declination angles after each AFD field (Figure 4). The declinations of the remaining samples vary by approximately ±20° (Figure 5A). The inclinations vary between -12° and -67° with an average of -40° (Figure 5B). The average inclination of -40° is about 20° greater than the expected axial dipole inclination at Laguna Cerritos Blancos. The higher-than-expected average inclination may be due to compaction of the top several tens of centimeters during coring.

The PSV record of LCB was correlated to that of ODP site 1233 (Lund et al., 2006) located at ~41°S latitude off the coast of Chile, (Figure 5C-D) by interpolating the age of each sample between 5 correlation points based on its depth. These correlation points were chosen based on the similarity of their inclination and declination angles to those of the ODP 1233 PSV record, marked on the PSV record in figures 5E and F. This correlation process dates the bottom

of this core at 4.0 kyr BP, ~500 years younger than the calibrated ^{14}C age model. The possible reasons for this are the freshwater reservoir effect or re-deposition of older organic matter into the lake. Some possible causes of the freshwater reservoir effect are a lake's low interaction with the atmosphere, which may be caused by long periods of snow cover; and discharge from meltwater originating from a glacier with an extended residence time (Philippsen, 2013). Furthermore, most organic matter in LCB is likely to have been redeposited considering that, presently, the lake is surrounded by very few plants and grasses, so organic matter would probably need to be moved multiple times with multiple storm events over hundreds of years in order to reach and deposit in the lake. Eglinton (2010) has demonstrated that lags of several hundred to several thousand years in terrestrial plant deposition is possible. For these reasons the PSV correlation age was preferred. The LCB PSV record probably represents a regionally significant PSV record because the ODP site 1233 PSV record has been correlated to 8 other PSV records throughout the southern hemisphere (Lisé-Pronovost et al., 2013).

5.1.2 Lithology

Two zones were recognized by the variations in grain size and geochemistry. Zone 1 spans ~4.0-2.2 cal kyr BP (1.37-0.94 mbgs) and Zone 2 spans ~2.2-0.05 cal kyr BP (0.94-0 mbgs) (Figure). The core is composed mainly of light brown/gray and orange colored fine sand-silty clay. On the Munsell Soil Color System, these colors correlate to variations between pale yellow and light brownish gray. Zone 1 contains orange silty clay-clayey silt transitioning to light brown/light gray from the bottom of the core to 1.1 mbgs. The rest of Zone 1 is composed of light brown/light gray clayey silt-silty clay. Zone 2 consists mostly of light brown/light gray silty clay-fine silt interlayered with silt-fine sand.

5.1.3 Grain Size Analysis

Grain-size analyses are recorded as the mean grain size of the bulk and coarse fraction (Figure A); bulk and coarse fraction grain-size populations (Figure B); and clay, silt, and sand percentages (Figure C). The LCB core is composed mostly of silt-sized sediment. Grain sizes increase up core while both the frequency and amplitude of grain-size variations also increase up core.

Zone 1 contains the smallest grains in the core and shows a gradual positive trend in bulk and coarse fraction mean grain size with an average grain size of 6.8 μm. Also, clay percent decreases while silt and sand percent increase slightly.

Zone 2 contains the largest grains of the core with an average of 20.1 μm, which vary widely with a standard deviation of 25.7 μm. Furthermore, the mean grain size of the coarse fraction deviates more often from the bulk mean grain size compared to Zone 1 with at least 12 samples measuring >50 μm, showing frequent high-amplitude variations. The silt and sand % show the same trend, with sand % increasing and silt % decreasing where high-amplitude variations occur.

5.1.4 Geochemistry

~20% of the LCB samples were analyzed for TIC at intervals of ~0.15 m. All samples were found to have <0.1% TIC with an average of 0.03%, which was considered negligible for the purposes of this study (Figure G). Thus, the total C, corresponding to the next analysis is considered to be equivalent to the TOC.

Very low C and N wt % values in Zone 1 of the core probably render the C/N ratios somewhat unreliable for interpretation in this zone, while greater C and N wt % values in Zone 2 make the C/N ratios reliable (Figure 6D-E).

Through Zone 1 the C and N weight percentages remain very low with averages of 0.31% and 0.04%, respectively. Zone 2 shows a general increase in C and N wt % having averages of 1.4% and 0.17%, respectively. This increase is accompanied by frequent high-amplitude variations reflected by an increase in standard deviation from Zone 1 to 2 in C and N wt %. The standard deviation of C wt % increases from Zone 1 to 2 by 0.5 to 0.7% and that of N wt % increases by 0.07 to 0.09% (Figure 6D-E). C/N ratios show a slight decrease through Zone 2, but remain largely constant with an average of 11.1 (Figure 6F).

5.1.5 Rock Magnetism

The volume- (κ) and mass- (χ) normalized low-field susceptibility, which is typically a measure of the concentration of magnetite, is low throughout the LCB core with averages of 9.0E-7 (SI) and 3.7E-10 m^3/kg, respectively. The greatest values are found within Zone 1 (Figure 6H-I). The susceptibility decreases through Zone 1, then nearly levels out going into Zone 2 to around values of 4.5E-7 (SI) and 1.5E-10 m^3/kg, respectively. Subsequently, frequent high-amplitude variations occur beginning about halfway through Zone 2 at ~0.85 mbgs (~1.2 cal kyr BP) through the end of the zone.

ARM_{20mT} and IRM_{20mT} data, which measure the concentration of high-coercivity grains show similar trends through the LCB core (Figure 6J-K). The ARM_{20mT} varies between 2.1E-3 and 6.7E-2 A/m, with an average of 8.6E-3 A/m, while IRM_{20mT} varies between 0.1 and 6.1 A/m, with an average of 0.75 A/m. These data decrease quickly by more than an order of magnitude from the bottom of the core until ~1.14 mbgs (~3.4 cal kyr BP), then remain close to their minimum values after this point through the rest of the core with an increase in the amplitude of variations beginning ~0.85 mbgs (~1.2 cal kyr BP) until the top of the core with local maxima of 0.01 and 2.4 A/m, respectively.

The IRM_{0mT}/ARM_{20mT} ratio which usually represents magnetic grain size, varies between 74 and 366 with an average of 146. Magnetic grain sizes are relatively large through Zone 1 with values ~150, decrease into Zone 2 to values ~105, then the amplitude and frequency of variations increases through Zone 2 (Figure 6L).

The S-ratio showing the relative proportion of magnetite to hematite, possesses values close to unity with an average of 0.86 (Figure 6M). HIRM, a measure of the absolute amount of hematite, varies between 8.0 and 0.2 A/m with an average of 1.2. The data show the greatest values residing at the bottom of the core, which decreases by an order of magnitude until ~1.14 mbgs (3.4 cal kyr BP). Increased values occur again after ~0.85 mbgs (~1.2 cal kyr BP) where the amplitude of variations increases with a local maximum of 4.0 A/m (Figure 6N).

The relative paleointensity (RPI) recorded as both NRM_{20mT}/ARM_{20mT} and NRM_{20mT}/IRM_{20mT} (Figure 7DE) correlates well with the RPI of ODP site 1233 (Figure 7F).

5.2 Laguna El Cepo

5.2.1 Age Control

Ages of charcoal samples were used, where available. The shallowest and deepest radiocarbon ages from the LEC core yield a sedimentation rate of ~0.4 m/kyr. Extrapolation on the 6 radiocarbon ages, dates the bottom of the core at 11 cal ^{14}C kyr BP (Figure 3). The LEC core was not used for PSV dating because all samples analyzed possessed undetectable or low-stability ChRMs.

5.2.2 Lithology

The lithology of the core is composed mostly of dark brown and olive silt-silty clay and is characterized by several thinly layered (<1 cm) sections that occur frequently. Zones 1-2 are composed mostly of medium to dark olive clayey silt and have thin layers that usually alternate

between medium olive and dark olive or brown. The beginning of Zones 3 until 2.2 cal kyr BP contains medium to very dark olive silty clay to very dark brown clayey silt and have thin layers that alternate between medium and dark olive. From 2.2 cal kyr BP until the end of Zone 3 consists mostly of dark brown silt-clayey silt and has thin layers that alternate between dark brown clayey silt and very dark brown silt.

Paleoclimate proxy data suggest three zones based on variations in grain size, C and N wt %, and C/N ratio throughout the LEC core. Zone 1 spans ~10.9-9.5 cal kyr BP (5.5-5.02 mbgs), Zone 2 ~9.5-5.5 cal kyr BP (5.02-3.26 mbgs), and Zone 3 ~5.5 cal kyr BP-present (3.26-0 mbgs) (Figure 8, 9).

5.2.3 Grain Size Analysis

Grain-size analyses are again recorded as bulk and coarse fraction mean grain size (Figure 8A), bulk and coarse fraction grain-size populations (Figure 8B), and clay, silt, and sand % in (Figure 8C). The core is dominated by silt-sized sediment and grain size generally increases up core. Zone 1 has a uniform grain size with an average bulk mean grain size of 10.3 µm and average coarse fraction mean grain size of 16.1 µm including only three bimodal samples or samples with greatly differing bulk and coarse fraction mean and population grain sizes. Zone 2 contains fine and constant grain sizes with an average bulk mean grain size of 12.1 µm and coarse fraction mean grain size of 15.9 µm showing decreased bimodality of grain size distributions. This zone is interrupted by a short period from ~8.3 to 7.7 cal kyr BP dominated by bimodal samples. Some of the coarse fraction populations of the bimodal samples within this short interval are as large as 720 µm. Silt percent is constantly high (90%) and clay (8.5%) and sand percent (1.4%) are low. Zone 3 contains predominantly bimodal samples with an average bulk mean grain size of 14.2 µm and coarse fraction mean grain size of 27.9 µm. The coarse

fraction populations are often >540 µm. Silt percent is slightly lower while clay and sand percentages are slightly higher throughout with averages of 80.5 %, 11.9 %, and 7.6 %, respectively. Zone 3 is interrupted by two short periods of decreased bimodality of grain-size distributions that occurred from ~4.9 to 4.4 cal kyr BP and ~2.6 to 2.2 cal kyr BP. The bulk mean and population grain sizes decrease slightly after 0.5 cal kyr BP.

5.2.4 Geochemistry

As was the case with the LCB core, the TIC of the LEC core was negligible. ~10% of the samples were analyzed for total inorganic carbon at intervals of ~0.21 m and every sample in this subset was found to have <0.1% TIC with an average of 0.03% (Figure 8G). Thus, the total C is considered to be equivalent to the TOC.

C/N ratios are relatively high through Zone 1 with several values >20 (Figure 8F). C and N wt % increase through Zone 1 (Figure 8D-E). C/N ratios increase from the beginning of Zone 2 until 7.7 cal kyr BP from ~10 to ~17. The interval from 7.7 cal kyr BP to the end of Zone 2 contains the lowest C and N wt % within the core and the C/N ratios decrease gradually from ~16 to ~10 with a few ratios >20. In Zone 3, C and N wt % increase slightly until ~4.0 cal kyr BP, while C/N ratios increase again to more than 16. At ~4.0 cal kyr BP there is a sharp increase in C and N wt % of about 14% and 1%, respectively, until ~3.8 cal kyr BP. After ~3.8 cal kyr BP, these decrease gradually until ~2.2 cal kyr BP. From ~4.0 to ~2.2 cal kyr BP, C/N ratios also decrease gradually with ratios as low as 3. C and N wt % increase again from ~2.2 cal kyr BP until present up to ~16% and ~1.6%, respectively, while C/N ratios vary consistently between ~9 and ~16. Furthermore, the C wt % and C/N ratio decrease slightly after 0.5 cal kyr BP (Figure 8D-F).

5.2.5 Rock Magnetism

The κ and χ susceptibilities were below the sensitivity of the Bartington MS2 susceptibility meter (Figure 9A-B). ARM_{20mT} and IRM_{20mT}, however, were detectable. ARM_{20mT} ranges in value between 1.15E-4 and 2.34E-3 A/m with an average of 4.29E-4 A/m. ARM_{20mT} values increase gradually, but steadily up core (Figure 9C). Superimposed on this quasi-linear increase are variations with periods of ~0.5 kyr (e.g., the >4E-4 A/m oscillation from 5.3 to 4.5 cal kyr BP), and ~0.2-0.3 kyr (e.g., the two 2E-4 A/m oscillations between 6.3 and 5.6 cal kyr BP).

The LEC IRM_{20mT} data (Figure 9D) range in value from 0.024-0.11 A/m and have an average value of 0.052 A/m. This record is dominated by the higher frequency oscillations noted in the ARM_{20mT} with a peak to peak amplitude of 0.03-0.04 A/m. The period of this oscillation decreases abruptly at ~1.8 cal ^{14}C kyr BP from ~200-500 years to ~100 years.

The IRM_{0mT}/ARM_{20mT} ratio through the LEC core (Figure 9E) varies between 61.4 and 754.6 and has an average of 285.4. These values are also dominated by higher frequency oscillations with an amplitude of ~200-600. These oscillations have a similar period to that of the IRM_{20mT} as expected. The S-ratio shows most values nearly equal to one, varying between 0.84 and 1.06 and averaging 1.0 (Figure 9F). The HIRM varies between 0.04 and 0.21 A/m with an average of 0.11 A/m and shows an almost exactly similar wavelength to the IRM_{20mT} (Figure 9G).

6. Discussion

6.1 Laguna Cerritos Blancos

6.1.1 Grain Size and Geochemistry

6.1.1.1 Zone 1: ~4.0-2.2 cal kyr BP (1.37-0.94 mbgs)

The fine and constant grain sizes lacking variation between the bulk and coarse fraction mean grain sizes (Figure 6A) and population grain sizes (Figure 6B) through Zone 1 indicate stable surface conditions caused by infrequent storm activity, suggesting dry climate conditions. Drier climate during this period is supported by low C and N wt % (Figure 6D-E) because these suggest low biological productivity.

6.1.1.2 Zone 2: ~2.2-0.05 cal kyr BP (0.94-0 mbgs)

Frequent high-amplitude variations in mean grain size (Figure 6A) and greater differences between grain-size populations (Figure 6B) suggest frequently changing surface conditions caused by frequent storm activity and wetter climate. Through Zone 2, C and N wt % (Figure 6D-E) increase gradually with wide variations indicating an increase in biological productivity caused by wetter conditions.

6.1.2 Rock magnetism

6.1.2.1 Zone 1: ~4.0-2.2 cal kyr BP (1.37-0.94 mbgs)

All magnetic concentration parameters (κ, χ, ARM_{20mT}, and IRM_{20mT}) (Figure 6H-K) show that the concentration of magnetic material in Zone 1 is relatively high and decreases until ~1.18 mbgs (~3.4 cal kyr BP) when higher-amplitude variations relative to Zone 1 occur (Evans and Heller, 2003). IRM_{0mT}/ARM_{20mT} ratios (Figure 6L) show relatively high values through this zone, which typically suggests that the magnetite grain size is relatively large (Evans and Heller, 2003). The S-ratio (Figure 6M) indicates that magnetite dominates the magnetization (Evans and

Heller, 2003), however the high HIRM values (Figure 6N) from the beginning of Zone 1 (1.37 mbgs) until 1.18 mbgs (~3.4 ^{14}C cal kyr BP) suggest that there is a large amount of hematite compared to <1.18 mbgs (Rosenbaum et al., 1996; Liu et al., 2007). The increased hematite and orange color in this same interval supports the interpretation that this time period (~4.0-3.4 cal kyr BP) was characterized by dry climate conditions because the presence of hematite is consistent with soil formation under oxidizing conditions, which occurs mainly during less stormy, dry periods (Veit, 1996).

K, χ, ARM_{20mT}, and IRM_{20mT} (Figure 6H-K) after 3.4 cal kyr BP (1.18 mbgs) until the end of Zone 1 show the lowest concentrations of magnetic material throughout the core. The S-ratio still indicates that the composition of most of the magnetic grains is magnetite, the IRM_{0mT}/ARM_{20mT} (Figure 6L) ratios suggest that their grain size is relatively small, and the HIRM (Figure 6N) indicates little hematite in the upper part of Zone1.

6.1.2.2 Zone 2: ~2.2-0.05 cal kyr BP (0.94-0 mbgs)

K and χ susceptibilities (Figure 6H-K) show the concentration of magnetic material to be increasing, but varying widely. ARM_{20mT} and IRM_{20mT} (Figure 6J-K) susceptibilities show that the concentration of magnetic material varies only slightly from that of the upper part of Zone 1. IRM_{0mT}/ARM_{20mT} ratios (Figure 6L) suggest that the magnetite grain size increases and varies widely up core. The S-ratio (Figure 6M) shows that the dominant magnetic mineral is magnetite, while the HIRM (Figure 6N) shows increased amounts of hematite in the upper part of Zone 2.

The reliability of the RPI record above 1.25 mbgs (~3.7 cal kyr BP) is supported by several rock magnetic observations. First, the dominant magnetic mineral is magnetite shown by an S-ratio close to unity (Figure 6M). Second, the ARM_{20mT} and IRM_{20mT}, two magnetic concentration parameters, do not vary by more than one order of magnitude throughout most of

the core (Figure 7B-C), and both normalization methods, the NRM_{20mT}/ARM_{20mT} ratio and the NRM_{20mT}/IRM_{20mT} ratio are consistent with each other throughout the entire core (Figure 7D-E). The LCB RPI correlates well with the ODP site 1233 RPI (Figure 7F). This correlation is consistent with the PSV-based age control model (Figure 5E-F).

6.2 Laguna El Cepo

6.2.1 Age Control

To a first order, bulk sediment and charcoal samples yielded the same ages (Figure 3). The midpoints of each 1σ range of bulk sediment and charcoal sample from the same core depth only differ by 30 to 300 cal ^{14}C yr BP, indicating that this lake does not have a significant freshwater reservoir effect. As expected, the bulk sediment samples were usually older than the charcoal samples.

6.2.2 Grain Size and Geochemistry

6.2.2.1 Zone 1: ~10.9-9.5 cal kyr BP (5.5-5.02 mbgs)

High C/N ratios (Figure 8F) and increasing C and N wt % (Figure 8D-E) suggest increased discharge and storm activity supporting increasing biological productivity associated with wet climate. Three bimodal grain-size distributions (Figure 8A-B) around 9.5 and 10.8 cal ^{14}C kyr BP support this interpretation.

6.2.2.2 Zone 2 ~9.5-5.5 cal kyr BP (5.02-4.23 mbgs)

This Zone is dominated by small mean grain sizes with unimodal grain-size distributions (Figure 8A-B) and low C/N ratios (Figure 8F) suggesting dry conditions relative to Zone 1. Also, low C and N wt % (Figure 8D-E) suggest that biological productivity was inhibited by reduced discharge.

Zone 2 is interrupted by an interval with frequent bimodal samples between ~8.3 and ~7.7 cal kyr BP occurring at the same time as decreased bulk mean grain size, increased coarse fraction mean grain size (Figure 8A-B), increased C and N wt % (Figure 8D-E) and C/N ratios (Figure 8F). This evidence strongly suggests that this short time period was characterized by increasing discharge as a result of very intense frequent storms, which supported a growing biological environment within the lake. This abrupt and intense event has been dated at a similar age to the 8.2 ka event that occurred in the northern hemisphere (Thomas et al., 2007). Although ^{14}C dates indicate the duration of this climate event in northern central Chile to be hundreds of years longer than the duration of the 8.2 ka event, the low resolution of ^{14}C dates in the LEC core probably date this event artificially longer than it actually was due to an increased rate of sedimentation that would have occurred as a result of increased storm activity during this period.

6.2.2.3 Zone 3 ~5.5 cal kyr BP-present (3.26-0 mbgs)

Zone 3 mainly consists of bimodal grain-size distributions (Figure 8A-B) suggesting increased frequency and intensity of storm activity relative to Zone 2. This zone is interrupted by two short dry periods implied by a decreased frequency of bimodal grain-size distributions from 4.9 to 4.4 cal kyr BP and 2.6 to 2.2 cal kyr BP. Also, low C and N wt % compared to those immediately following each of these dry periods support this interpretation.

Before 4.9 cal kyr BP, slightly increasing C and N wt % (Figure 8D-E) indicate increasing biological productivity, while C/N ratios (Figure 8F) show increasing discharge, suggesting that conditions are becoming gradually wetter. After the first short dry period, large increases in coarse fraction grain size, C and N wt %, and C/N ratio suggest an intense increase in moisture ~4.0 cal kyr BP and probably represents the maximum amount of moisture and biological productivity occurring during Zone 3. After ~3.8 cal kyr BP these proxies decrease

until the most recent dry period. Afterwards, the increases in bimodality of grain-size distributions and C and N wt % suggest increasing storm activity supporting increasing biological productivity. Slight decreases in bulk mean grain size, C wt %, and C/N ratios after ~0.3 cal ^{14}C kyr BP (Figure 8) suggest a drying trend that is probably associated with the current dry climate conditions in the region.

6.2.3 Rock magnetism

Undetectable low-field susceptibility (Figure 9A-B) suggests a very low concentration of magnetic grains in the LEC core. However, ARM_{20mT} and IRM_{20mT} susceptibilities (Figure 9C-D) indicate presence of variations in the concentration of high-coercivity magnetite grains. ARM_{20mT} increases gradually and slightly up core, which is a similar trend to that of the bulk and coarse fraction mean grain sizes. The reason for this trend could be that magnetite has been better preserved over time due to increasing storm activity through the Holocene that caused increasing lake depth and anoxic conditions that preserve magnetite crystals. The S-ratio shows that the dominant magnetic mineral in the core is magnetite, while HIRM suggests the presence of hematite varies uniformly, periodically by ~200-500 years. IRM_{20mT} shows the exact same wavelength indicating that hematite resides only where magnetite is relatively abundant in this core. The IRM_{0mT}/ARM_{20mT} has the same wavelength as the HIRM, suggesting that the grain size of magnetite grains varies consistently with changes in the amount of high-coercivity minerals, such as hematite. This regular wavelength is consistent with the significantly thin, alternating layers, characteristic of the lithology of the LEC core. The ARM_{20mT}, IRM_{20mT}, IRM_{0mT}/ARM_{20mT}, and HIRM time series, were sampled at 2-cm intervals, significantly longer than the ≤1-cm wavelength of the lithologic layers. Thus, the magnetic proxies may be aliased versions of the lithologic variations.

6.3 Regional Holocene Paleoclimate

This paleoclimate record correlates well with other records in the region, including that of Maldonado and Villagrán (2006) (Figure 10). The wet period from ~10.9-9.5 cal kyr BP in LEC correlates with the wet period from 9.9-8.7 cal kyr BP. The dry periods from ~9.5-8.3 cal kyr BP and ~7.7-5.5 cal kyr BP in LEC correlate with the arid period from 7.8 to 5.7 cal kyr BP in Maldonado and Villagrán (2006). The wet period ~8.3-7.7 cal kyr BP from LEC is not consistent with the Maldonado and Villagrán (2006) record. The wet periods ~5.5-4.9 cal kyr BP and ~4.4-2.6 cal kyr BP correlate to the wet period from 5.7 to 3.0 cal kyr BP in Maldonado and Villagrán (2006), however the dry period ~4.9-4.4 cal kyr BP from LEC is not consistent with this record. The mildly dry period 3.0-2.2 cal kyr BP from Maldonado and Villagrán (2006) correlates with the dry periods 2.6-2.2 cal kyr BP in the LEC core and 4.0-2.2 cal kyr BP in the LCB core. The humid phase with variable moisture 2.2 cal kyr BP-present correlates well with the same time period of similar conditions found in both LCB and LEC cores.

The paleoclimate record built by Veit (1996) also correlates well with this paleoclimate record (Figure 10). His wet period in the early Holocene until 7.3 cal kyr BP correlates with the wet periods ~10.9-9.5 and ~8.3-7.7 cal kyr BP from the LEC core, however the dry period from ~9.5-8.3 cal kyr BP is not consistent with the record from Veit (1996). The dry period 7.3-5.1 cal kyr BP correlates with the dry period ~7.7-5.5 cal kyr BP in the LEC core. The wet period from 5.1 to 3.7 cal kyr BP of Veit (1996) correlates with the wet periods ~5.5-4.9 cal kyr BP and ~4.4-2.6 cal kyr BP. The dry period ~4.9-4.4 cal kyr BP is not consistent with the Veit (1996) record. The dry period 3.7-3.0 cal kyr BP correlates with the dry period 2.6-2.2 cal kyr BP from LEC and the dry period from 4.0-2.2 cal kyr BP from LCB. The period of varying precipitation after

3.0 cal kyr BP from Veit (1996) correlates with the wet period 2.2 cal kyr BP-present found in LCB and LEC cores.

Any discrepancies among these records is probably due to their differences in location or to inaccuracies generally expected from radiocarbon dating.

6.4 Implications

Large-scale changes in climate in this region are caused by variations in strength and movement of the westerly winds (causing wet climate) and the SPA (causing dry climate) (Garreaud, 2009; Maldonado and Villagrán, 2006; Veit,1996). Evidence from LEC suggests that the westerlies were dominant in northern central Chile ~10.9-9.5 cal kyr BP, then moved slightly southward ~9.5-8.3 cal kyr BP. ~8.3-7.7 cal yr BP the westerlies abruptly moved north. They began moving south again around 7.7 cal kyr BP and remained south with the SPA possibly strengthened until ~5.5 cal kyr BP when the westerlies began moving northward gradually and/or the SPA weakened gradually. Consistent with the previous conditions, the westerlies became much stronger and/or moved far to the north beginning ~4.0 cal kyr BP. Then evidence from LEC and LCB suggests that the westerlies began moving gradually southward ~3.8 cal kyr BP until ~2.2 cal kyr BP when they began moving gradually northward and probably shifted direction again ~0.05 cal kyr BP causing the dry climate conditions today in Norte Chico.

6.5 Global Holocene Paleoclimate

Periods of intense storm activity found in LCB and LEC cores roughly correlate with periods of rapid climate change (RCC) found in paleoclimate records globally. Mayewski et al. (2004) hypothesized 6 periods of rapid climate change based on ~50 globally distributed paleoclimate records: 9.0-8.0; 6.0-5.0; 4.2-3.8; 3.5-2.5; 1.2-1.0; and 0.6-0.15 kyr BP. These periods mostly exhibit anomalously cool polar regions and dry tropics, furthermore 9.0-8.0 kyr

BP is associated with the 8.2 ka event and the interval from 0.6-0.15 kyr BP is unique because it is associated with cool poles and wet tropics.

The time periods of discrete climate changes in LCB and LEC, identified based on grain size, C and N wt %, and C/N ratio, that may correspond to these hypothesized periods of global RCC include 8.3-7.7, 5.5-5.0, 4.0-3.8, and 1.2-1.0 cal kyr BP. Figure 11 shows the hypothesized periods of RCC (Mayewski et al., 2004) as shaded rectangles superimposed on the LEC grain-size population record due to the obvious changes between unimodal and bimodal samples. The first period of increased storm activity 8.3-7.7 cal kyr BP suggested by the sharp increase in grain-size bimodality in the LEC core record is roughly similar to the period 9.0-8.0 kyr BP. This period of increased storm activity includes the 8.2 ka event, a short period of global cooling caused by a massive influx of freshwater into the Hudson Bay (Thomas et al., 2007) at ~8.2 ka. Another stormy period 5.5-5.0 cal kyr BP correlates with the RCC period 6.0-5.0 kyr BP. A sharp increase in moisture associated with storm activity 4.0-3.8 cal kyr BP found in LEC also correlates with the RCC period 4.2-3.8 kyr BP. The period 3.5-2.5 kyr BP in northern central Chile was dry, as indicated by small grain sizes in LCB and LEC during this period, but is not a period of rapid or drastic change in climate conditions. 1.2-1.0 kyr BP was a period of moderately abrupt climate change in Norte Chico when climate shifted from a mildly dry period to a period of more frequent storm activity. The final RCC period 0.6-0.15 kyr BP does not correlate to any discrete climate changes in northern Chile. The predominance of correlations described above suggest that northern central Chile may ultimately be affected by global climate drivers throughout most of the Holocene.

7. Conclusion

The paleoclimate record recovered from the LCB and LEC cores suggest the following for the Holocene Epoch in the region of central Chile: The climate in this time period begins with a wet period ~10.9-9.5 cal kyr BP, that transitions to a short dry period ~9.5-8.3 cal kyr BP caused by northward then southward shifts of the westerlies. The westerlies again shift northward quickly, suggested by an abrupt increase in storm activity from ~8.3-7.7 cal kyr BP. The driest period in northern central Chile, possibly due to a substantial southward displacement of the westerlies, occurred from ~7.7 to 5.5 cal kyr BP. The westerlies then began to move northward slightly, but was weakly affecting the study area from ~4.9-4.4 cal kyr BP causing dry conditions. Subsequently, moisture increased and reached a maximum at 4.0 cal kyr BP as a result of an abrupt northward shift of the westerlies. After ~3.8 cal kyr BP the westerlies moved south gradually, causing moisture and storm activity to decrease gradually causing dry conditions from ~2.6 until 2.2 cal kyr BP when they shifted northward causing gradually increasing moisture and more frequent storm activity.

This record is consistent with other paleoclimate records in the region (Veit, 1996; Maldonado and Villagrán, 2006 and references within). Finally, its overall correlation with global Holocene climate records suggests that climate change in northern central Chile responds quickly to drivers of global climate change.

References

Acton, G., ZPLOTIT Software v2009-10. Downloaded from http://paleomag.ucdavis.edu/software-Zplotit.html, 2009.

Acton, G., ZPLOTIT Software Users' Guide Version, version 2009-10, Downloaded from http://paleomag.ucdavis.edu/software-Zplotit.html, 2009.

Blunt, A.B., Negrini, R.M., 2015. Lake levels for the past 19,000 years from the TL05-4 cores, Tulare Lake, California, USA, Geophysical and geochemical proxies. Quaternary International 387, 122-130, doi: 10.1016/j.quaint.2015.07.001.

Butler, R.F., 1992. Paleomagnetism: magnetic domains to geologic terranes. Blackwell Scientific Publications, Boston.

Cohen, A.S., 2003. Paleolimnology: The History and Evolution of Lake Systems. Oxford University Press, New York, NY. pp. 252-254.

Eglinton, T.I., 2010. Links between climate and transmission times of biomarker signals to aquatic sediments: Implications for interpretation of the sedimentary record. Abstract PP42A-03 presented at 2010 Fall Meeting, AGU, San Francisco, Calif., 13-17 Dec.

Evans, M.E., Heller, F., 2003. Environmental Magnetism: Principles and Applications of Enviromagnetics. Academic Press, San Diego, CA, pp. 21-22.

Ezilon Maps, 2015. South American Map – Physical Map of South America. http://www.ezilon.com/maps/south-america-physical-maps.html (accessed May 2016).

Garreaud, R.D., 2009. The Andes climate and weather. Advances in Geosciences 22, 3-11.

Kirby, M.E., Zimmerman, S.R.H., Patterson, W.P., Rivera, J.J., 2012. A 9170-year record of decadal-to-multi-centennial scale pluvial episodes from the coastal Southwest United States:a role for atmospheric rivers?. Quaternary Science Reviews 46, 57-65, doi: 10.1016/j.quascirev.2012.05.008.

Lisé-Pronovost, A., St-Onge, G., Gogorza, C., Haberzettl, T., Preda, M., Kliem, P., Francus, P., Zolitschka, B., The PASADO Science Team, 2013. High-resolution paleomagnetic secular variations and relative paleointensity since the Late Pleistocene in South America. Quaternary Science Reviews 71, 91-108, doi:10.1016/j.quascirev.2012.05.012.

Liu, Q., Roberts, A.P., Torrent, J., Horng, C., Larrasoaña, J.C., 2007. What do the HIRM and S-ratio really measure in environmental magnetism?. Geochemistry, Geophysics, Geosystems 8 (9), Q09011, doi:10.1029/2007GC001717.

Lund, S.P., Stoner, J., and Lamy, F., 2006. Late Quarternary paleomagnetic secular variation and chronostratigraphy from ODP Sites 1233 and 1234. *In Tiedemann, R.*, Mix, A.C., Richter, C., and Ruddiman, W.F. (Eds.), *Proc. ODP, Sci. Results, 202:* College Station, TX (Ocean Drilling Program), 1–22. doi:10.2973/ odp.proc.sr.202.208.2006.

Maldonado, A., Villagrán, C., 2006. Climate variability over the last 9900 cal yr BP from a swamp forest pollen record along the semiarid coast of Chile. Quaternary Research 66, 246-258, doi:10.1016/j.yqres.2006.04.003.

Mayewski, P.A., Rohling, E.E., Stager, J.C., Karlén, W., Maasch, K.A., Meeker, L.D., Meyerson, E.A., Gasse, F., Kreveld, S., Holmgren, K., Lee-Thorp, J., Rosqvist, G., Rack, F., Staubwasser, M., Schneider, R.R., Steig, E.J., 2004. Holocene climate variability. Quaternary Research 62, 243-255, doi:10.1016/j.yqres.2004.07.001.

McFadden, M.A., Patterson, W.P., Mullins, H.T., Anderson, W.T., 2005. Multi-proxy approach to long- and short-term Holocene climate-change: evidence from eastern Lake Ontario. Journal of Paleolimnology 33, 371-391.

Meyers, P.A., Lallier-Vergès, E., 1999. Lacustrine sedimentary organic matter records of Late Quaternary paleoclimates. Journal of Paleolimnology 21, 345-372.

Meza, F.J., 2013. Recent trends and ENSO influence on drought in Northern Chile: An application of the Standardized Precipitation Evapotranspiration Index. Weather and Climate Extremes 1, 51-58, http://dx.doi.org/10.1016/j.wace.2013.07.002.

Mpodozis, C., Kay, S.M., 1992. Late Paleozoic to Triassic evolution of the Gondwana margin: Evidence from Chilean Frontal Cordilleran batholiths (28°S to 31°S). Geological Society of America Bulletin 104, 999-1014.

Oyarzún, J., Carvajal, M.J., Maturana, H., Núñez, J., Kretschmer, N., Amezaga, J.M., Rötting, T.S., Strauch, G., Thyne, G., Oyarzún, R., 2013. Hydrochemical and isotopic patterns in a calc-alkaline Cu- and Au-rich arid Andean basin: The Elqui River watershed, North Central Chile. Applied Geochemistry 33, 50-63, http://dx.doi.org/10.1016/j.apgeochem.2013.01.014.

Philippsen, B., 2013. The freshwater reservoir effect in radiocarbon dating. Heritage Science 1 (24), 1-19, doi: 10.1186/2050-7445-1-24.

Rosenbaum, J.G., Reynolds, R.L., Adam, D.P., Drexler, J., Sarna-Wojcicki, A.M., Whitney, G.C., 1996. Record of middle Pleistocene climate change from Buck Lake, Cascade Range, southern Oregon – Evidence from sediment magnetism, trace-element geochemistry, and pollen. Geological Society of America Bulletin 108 (10), 1328-1341.

Sperazza, M., Moore, J.N., Hendrix, M.S., 2004. High-resolution particle size analysis of naturally occurring very fine-grained sediment through laser diffractometry. Journal of Sedimentary Research 74 (5), 736-743.

Stuiver, M., Reimer, P.J., 1993. Extended 14C data base and revised CALIB 3.0 ^{14}C age calibration program. Radiocarbon 35, 215-230.

Thomas, E.R., Wolff, E.W., Mulvaney, R., Steffensen, J.P., Johnsen, S.J., Arrowsmith, C., White, J.W.C., Vaughn, B., Popp, T., 2007. The 8.2 ka event from Greenland ice cores. Quaternary Science Reviews 26, 70-81, doi:10.1016/j.quascirev.2006.07.017.

Veit, H., 1996. Southern Westerlies during the Holocene deduced from geomorphological and pedological studies in the Norte Chico, Northern Chile (27-33°S). Palaeogeography, Palaeoclimatology, Palaeoecology 123, 107-119.

Zijderveld, J.D.A., 1967. AC demagnetization of rocks: analysis of results. Methods in Paleomagnetism 3, 254-286.

List of Figures

Figures

Figure 1

Figure 2

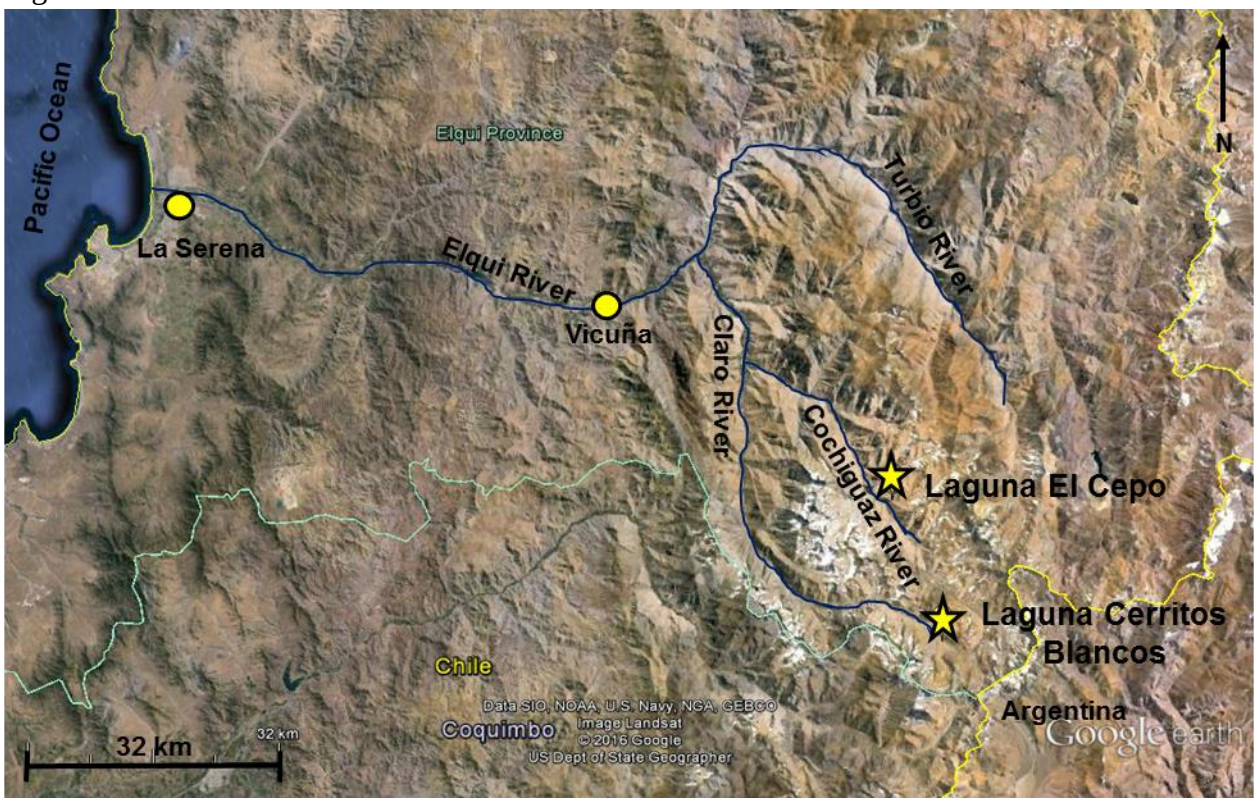
Pacific Ocean
Elqui Province
N
La Serena
Elqui River
Vicuña
Turbio River
Claro River
Cochiguaz River
Laguna El Cepo
Laguna Cerritos Blancos
Chile
Argentina
Coquimbo
Data SIO, NOAA, U.S. Navy, NGA, GEBCO
Image Landsat
© 2015 Google
US Dept of State Geographer
32 km
32 km
Google earth

Table 1

Sample Name	Sample Description	Depth Interval (m)	Depth Interval Midpoint (m)	^{14}C Age BP	±	1σ ranges (cal yr BP)	1σ range Midpoint (cal yr BP)
LCB-0114-AT1- 12-13	bulk sediment	0.12-0.13	0.125	790	30	664-688 703-719	691.5
LCB-0114-AT1- 40-41	bulk sediment	0.4-0.41	0.405	1350	30	1185-1219 1232-1249	1231
LCB-0114-AT2- 21-22	bulk sediment	0.74-0.75	0.745	2135	40	2010-2101 2131-2144	2077
LCB-0114-AT4- 6-7	bulk sediment	1.09-1.1	1.095	3430	120	3479-3729 3747-3767 3791-3824	3651.5
LEC-0114-AT1- 72-73	charcoal	0.72-0.73	0.725	880	90	673-804 871-898	785.5
LEC-0114-AT1- 72-73	bulk sediment	0.72-0.73	0.725	655	30	555-569 594-635	595
LEC-0114-AT2- 60-61	charcoal	1.51-1.52	1.515	1785	30	1611-1680 1691-1703	1657
LEC-0114-AT2- 60-61	bulk sediment	1.51-1.52	1.515	2085	35	1933-1968 1991-2053	1993
LEC-0114-AT3- 70-71	charcoal	2.59-2.6	2.595	3750	60	3934-3938 3971-4104 4106-4149	4041.5
LEC-0114-AT3- 70-71	bulk sediment	2.59-2.6	2.595	3940	40	4259-4265 4287-4414	4336.5
LEC-0114-AT5- 57-58	charcoal	4.12-4.13	4.125	6780	80	7516-7537 7562-7669	7592.5
LEC-0114-AT5- 57-58	bulk sediment	4.12-4.13	4.125	6810	30	7588-7626 7633-7655	7621.5
LEC-0114-AT5- 95-96	bulk sediment	4.5-4.51	4.505	7510	30	8210-8261 8294-8347	8278.5
LEC-0114-AT6- 92-93	bulk sediment	5.45-5.46	5.455	9535	50	10608-10614 10658-10793 10964-11005 11023-11065	10836.5

Figure 3

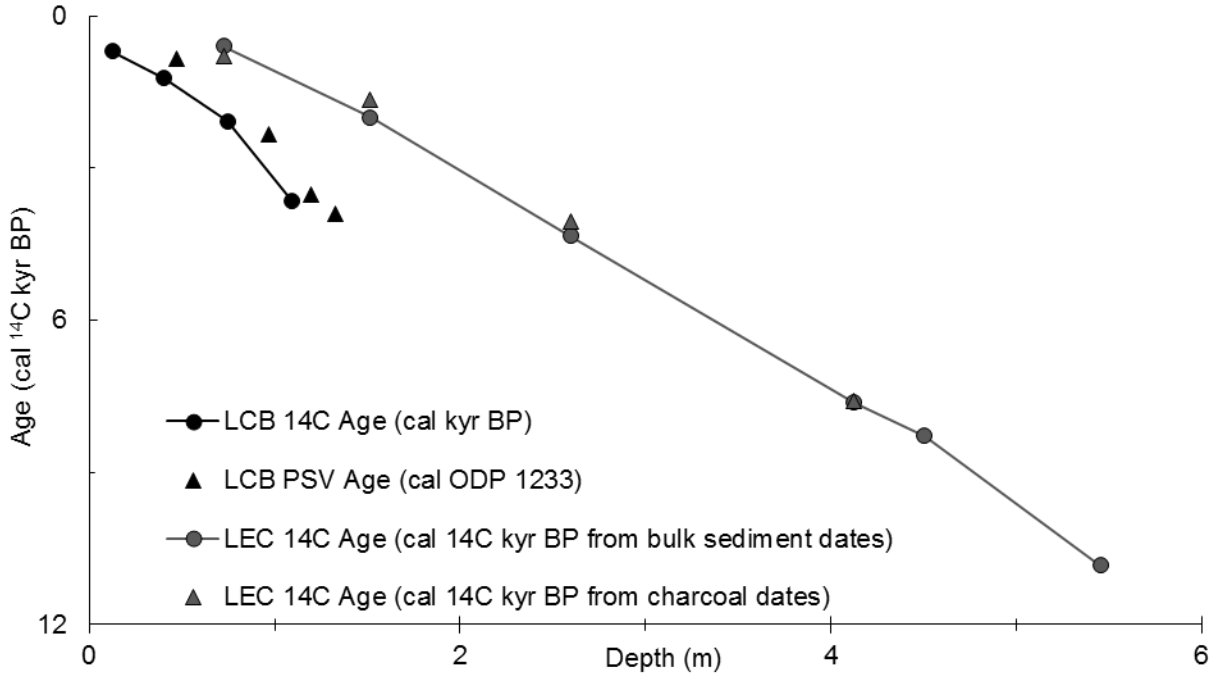
0
6
12
Age (cal ^{14}C kyr BP)
LCB 14C Age (cal kyr BP)
LCB PSV Age (cal ODP 1233)
LEC 14C Age (cal 14C kyr BP from bulk sediment dates)
LEC 14C Age (cal 14C kyr BP from charcoal dates)
0
2
4
6
Depth (m)

Figure 4

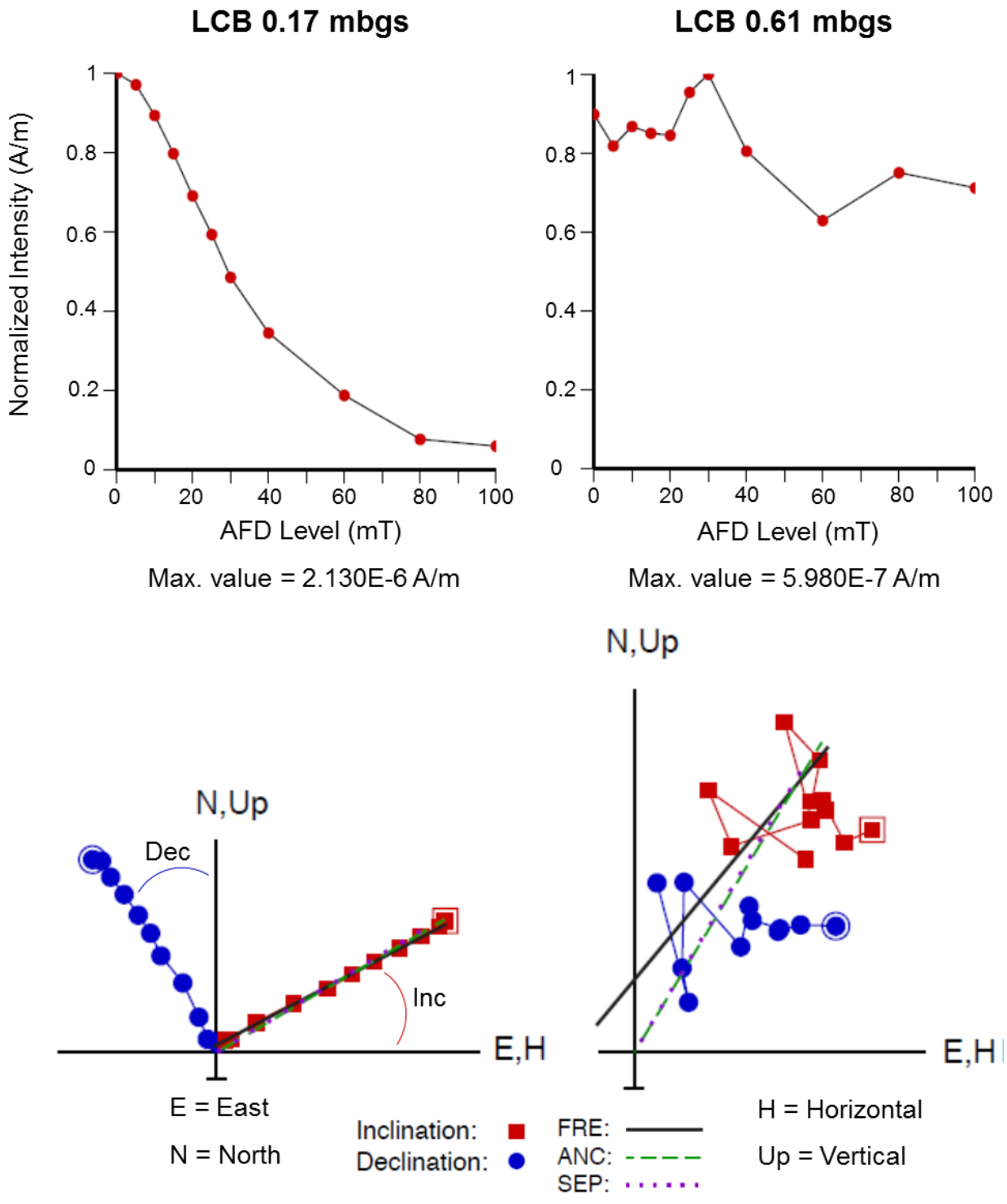
LCB 0.17 mbgs
LCB 0.61 mbgs
Normalized Intensity (A/m)
AFD Level (mT)
AFD Level (mT)
Max. value = 2.130E-6 A/m
Max. value = 5.980E-7 A/m
N,Up
Dec
Inc
E,H
N,Up
E,H
E = East
N = North
Inclination:
Declination:
FRE:
ANC:
SEP:
H = Horizontal
Up = Vertical

Figure 5

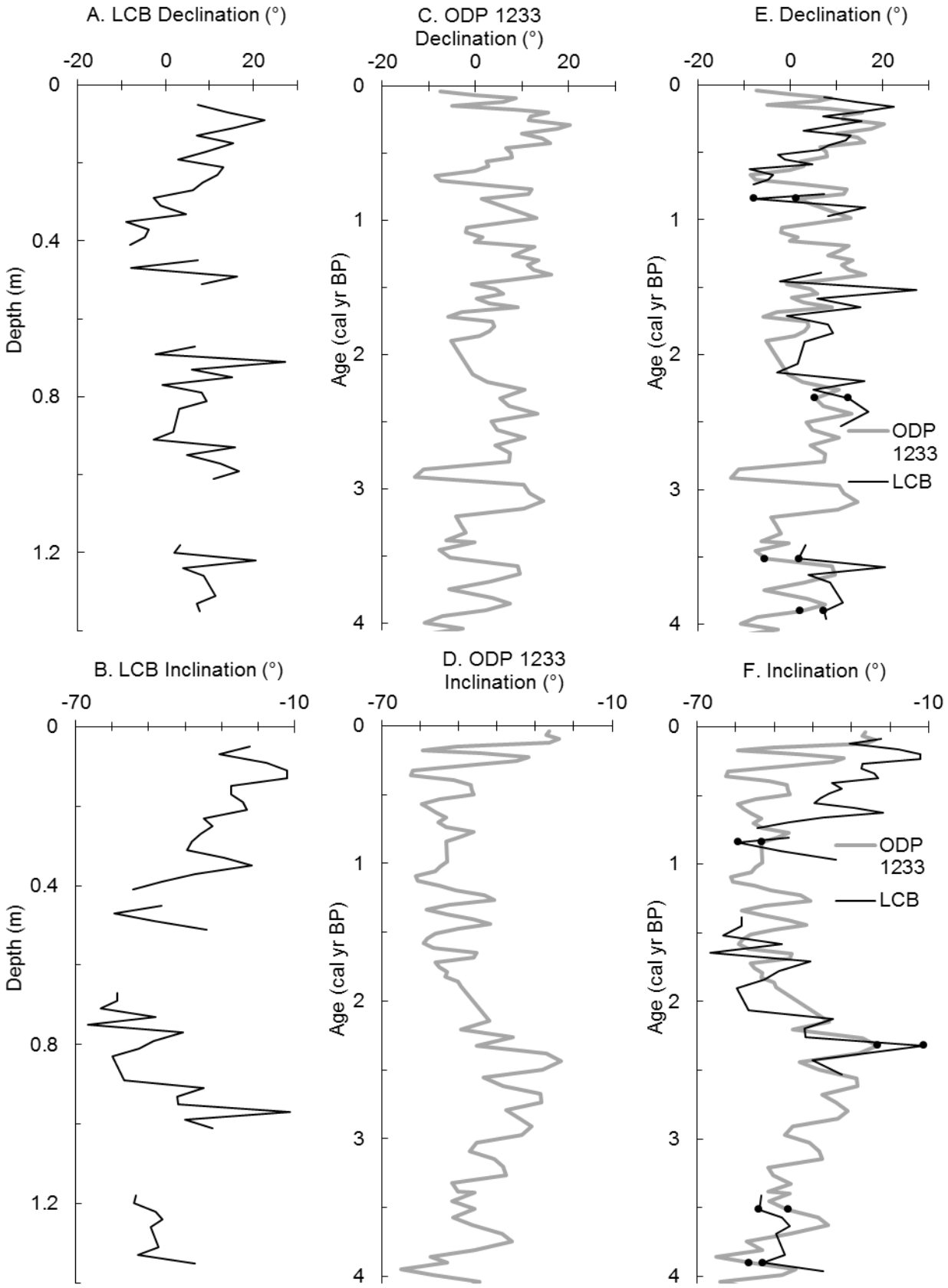
A. LCB Declination (°)
-20
0
20
0
0.4
0.8
1.2
Depth (m)
C. ODP 1233
Declination (°)
-20
0
20
0
1
2
3
4
Age (cal yr BP)
E. Declination (°)
-20
0
20
0
1
2
3
4
Age (cal yr BP)
ODP
1233
LCB
B. LCB Inclination (°)
-70
-10
0
0.4
0.8
1.2
Depth (m)
D. ODP 1233
Inclination (°)
-70
-10
0
1
2
3
4
Age (cal yr BP)
F. Inclination (°)
-70
-10
0
1
2
3
4
Age (cal yr BP)
ODP
1233
LCB

Figure 6

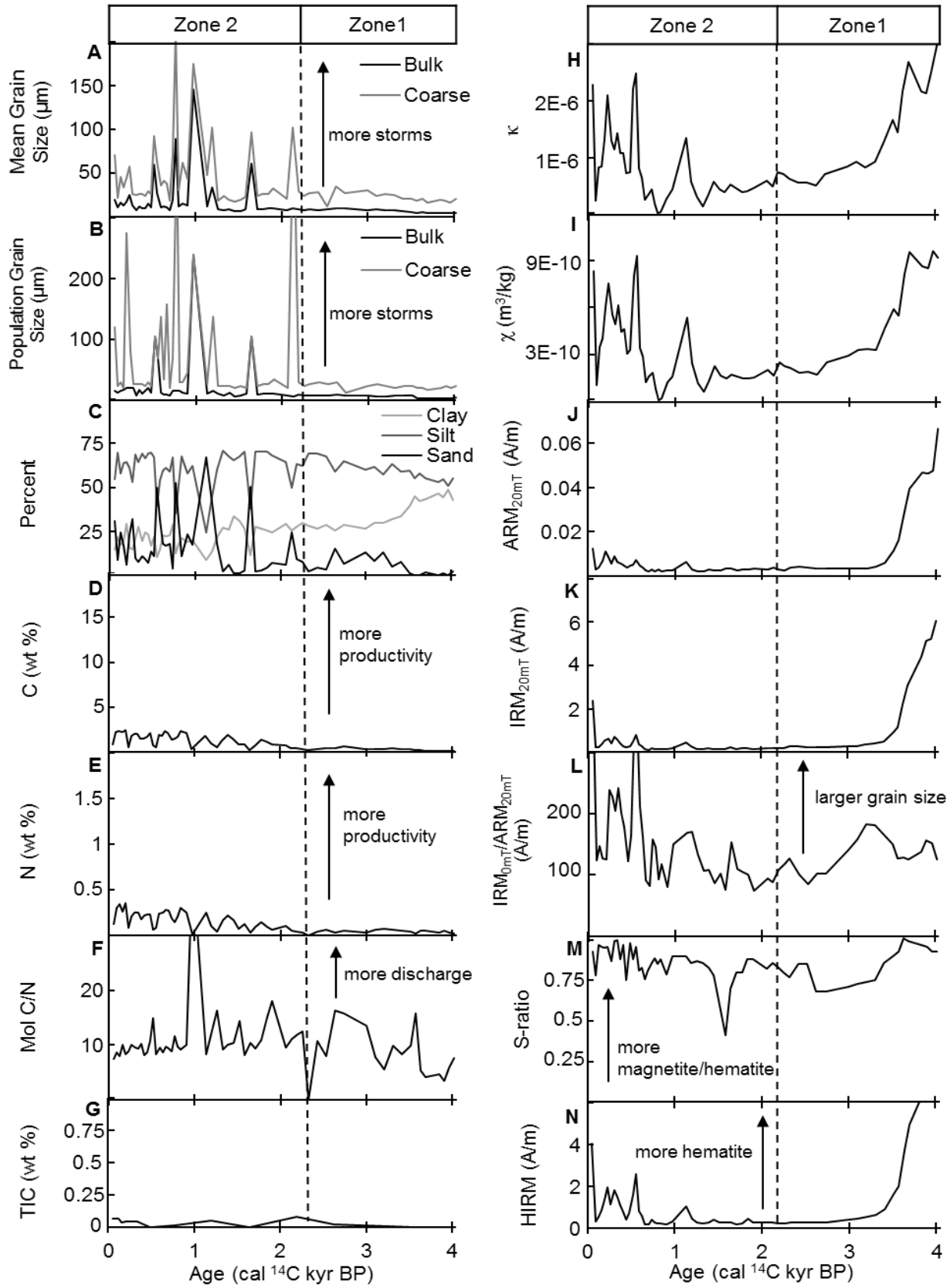
Zone 2
Zone1
A
Mean Grain Size (µm)
Bulk
Coarse
more storms
B
Population Grain Size (µm)
C
Percent
Clay
Silt
Sand
D
C (wt %)
more productivity
E
N (wt %)
F
Mol C/N
more discharge
G
TIC (wt %)
Age (cal 14C kyr BP)
H
κ
I
χ (m3/kg)
J
ARM20mT (A/m)
K
IRM20mT (A/m)
L
IRM0mT/ARM20mT (A/m)
larger grain size
M
S-ratio
more magnetite/hematite
N
HIRM (A/m)
more hematite

Figure 7

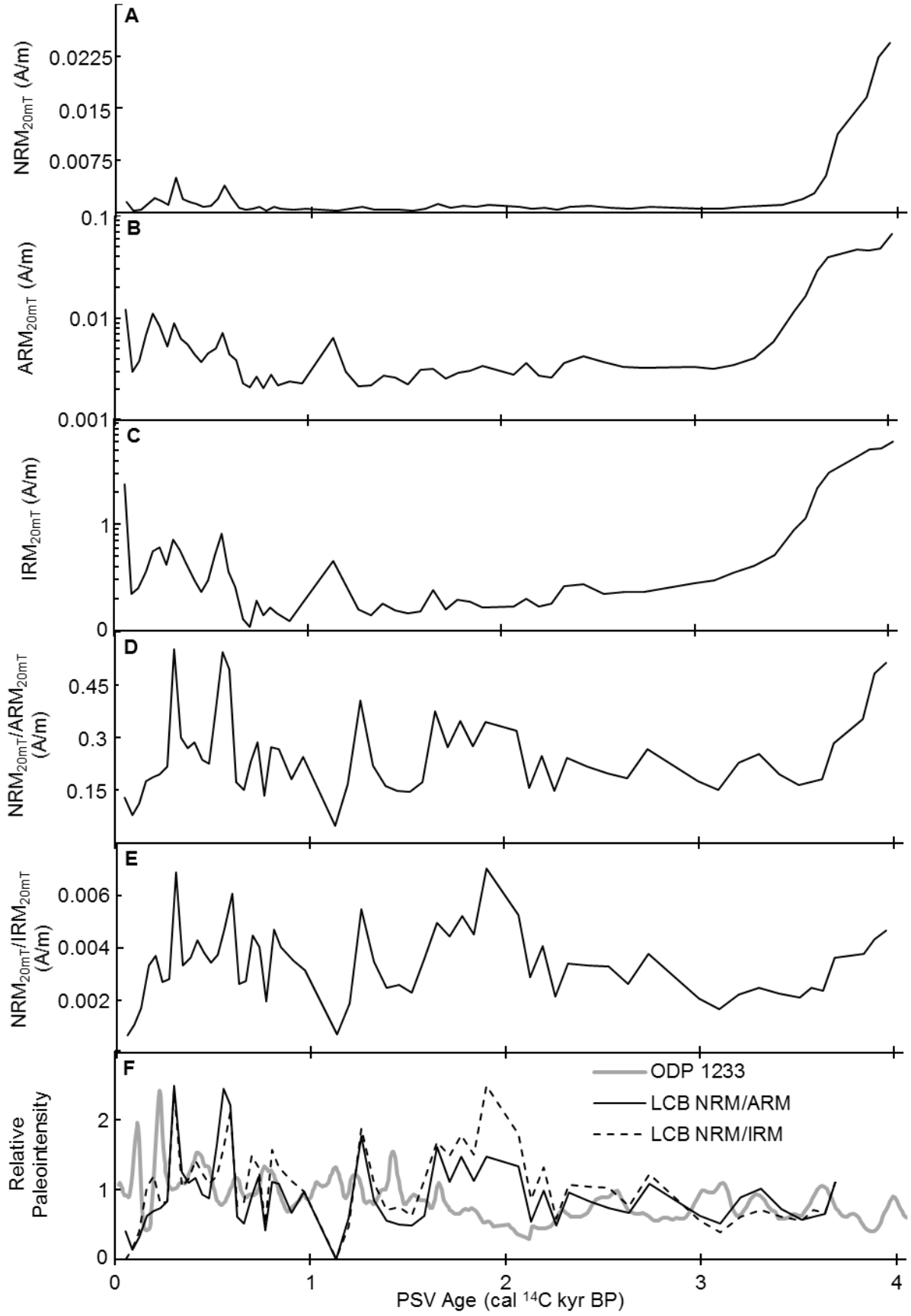
A
B
C
D
E
F
NRM20mT (A/m)
0.0225
0.015
0.0075
0.1
ARM20mT (A/m)
0.01
0.001
IRM20mT (A/m)
1
0
NRM20mT/ARM20mT (A/m)
0.45
0.3
0.15
NRM20mT/IRM20mT (A/m)
0.006
0.004
0.002
Relative Paleointensity
2
1
0
ODP 1233
LCB NRM/ARM
LCB NRM/IRM
0
1
2
3
4
PSV Age (cal 14C kyr BP)

Figure 8

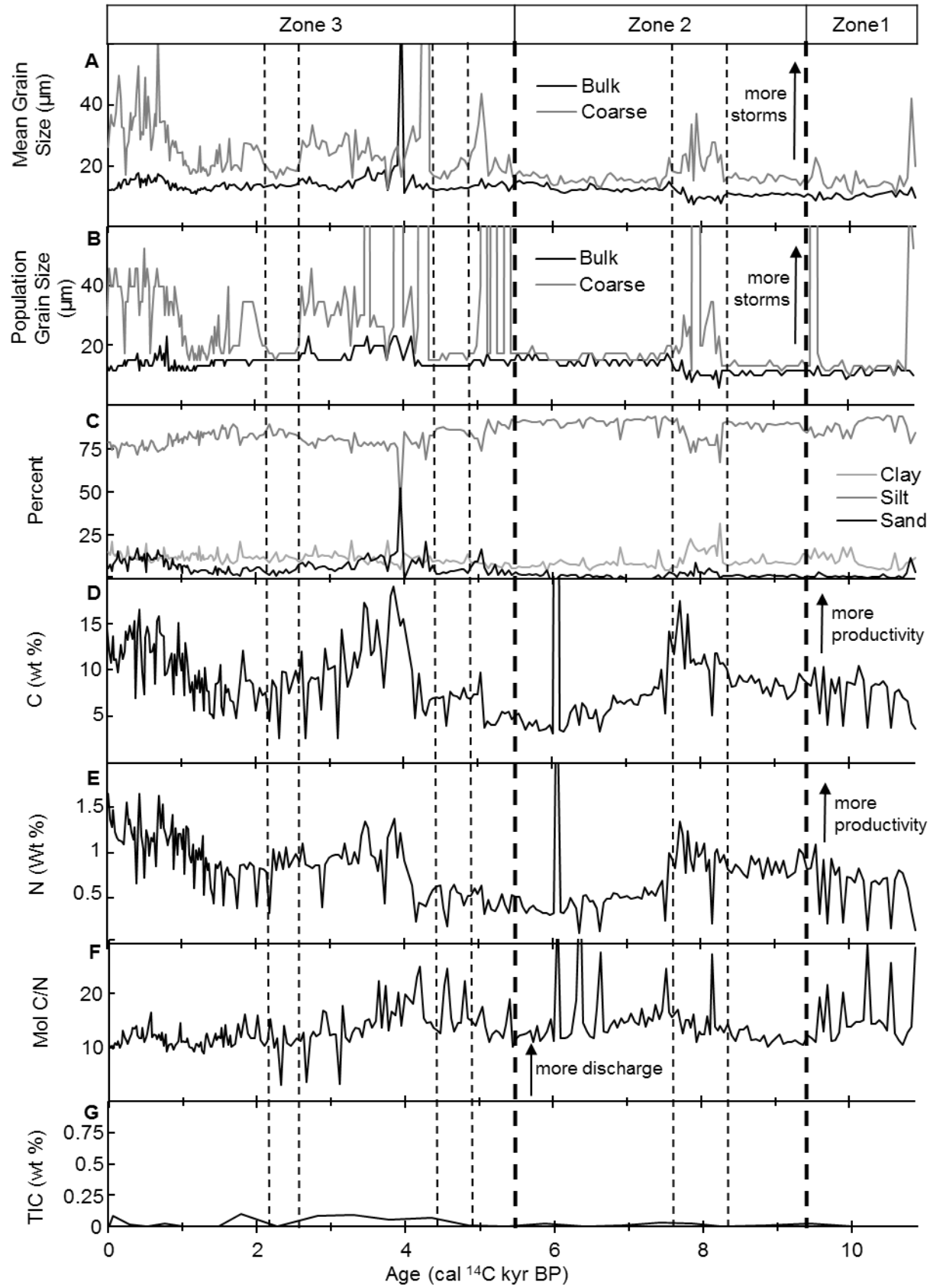
Zone 3
Zone 2
Zone1
A
Mean Grain Size (µm)
40
20
Bulk
Coarse
more storms
B
Population Grain Size (µm)
40
20
Bulk
Coarse
more storms
C
Percent
75
50
25
Clay
Silt
Sand
D
C (wt %)
15
10
5
more productivity
E
N (Wt %)
1.5
1
0.5
more productivity
F
Mol C/N
20
10
more discharge
G
TIC (wt %)
0.75
0.5
0.25
0
0
2
4
6
8
10
Age (cal 14C kyr BP)

Figure 9

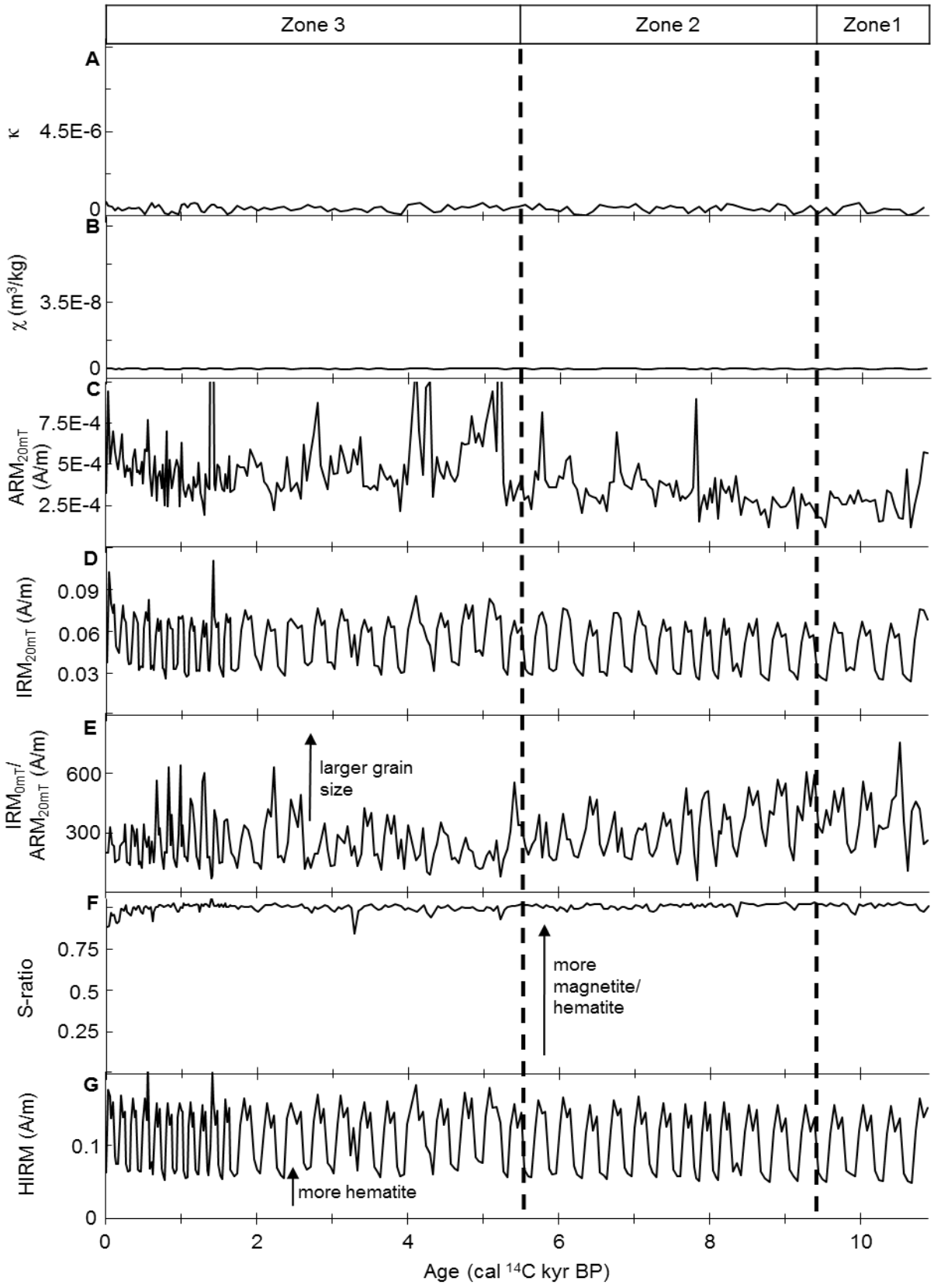
Zone 3
Zone 2
Zone1
A
κ
4.5E-6
0
B
χ (m³/kg)
3.5E-8
0
C
ARM20mT (A/m)
7.5E-4
5E-4
2.5E-4
D
IRM20mT (A/m)
0.09
0.06
0.03
E
IRM0mT/ ARM20mT (A/m)
600
300
larger grain size
F
S-ratio
0.75
0.5
0.25
more magnetite/ hematite
G
HIRM (A/m)
0.1
0
more hematite
0
2
4
6
8
10
Age (cal 14C kyr BP)

Figure 10

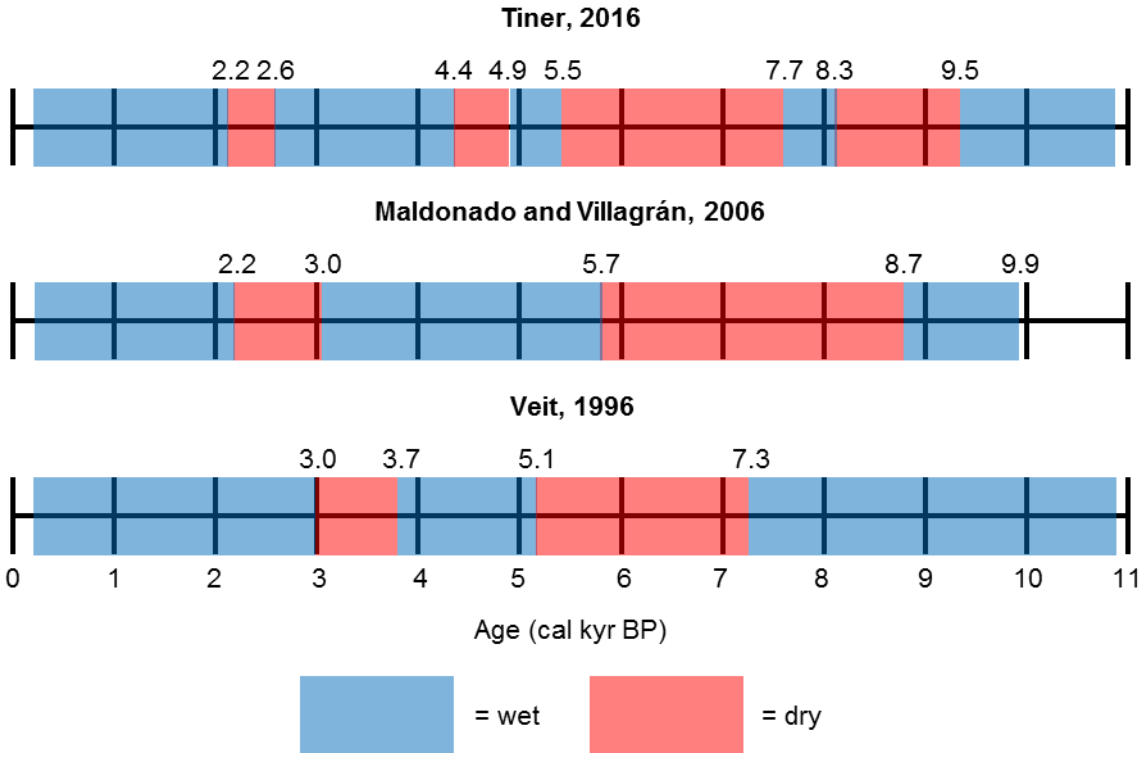

Figure 11